

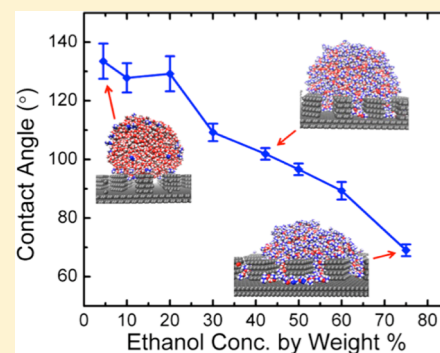
Wetting Transition of the Ethanol–Water Droplet on Smooth and Textured Surfaces

Atanu K. Metya, Sandip Khan, and Jayant K. Singh*

Department of Chemical Engineering, Indian Institute of Technology Kanpur, Kanpur 208016, India

Supporting Information

ABSTRACT: The wetting behavior of an ethanol–water droplet is investigated on graphitic smooth and rough surfaces using molecular dynamics simulations. On a smooth surface, ethanol molecules prefer to stay at the vapor–liquid and solid–liquid interfaces. The contact angle of a droplet on a smooth surface decreases with an increase in the ethanol concentration from 0 to 30 wt %. The corresponding line tension increases from 3×10^{-11} to 9.4×10^{-11} N at 300 K. The critical weight percentage for complete wetting is found to be approximately 50%. In the case of a textured graphite surface, with the addition of ethanol molecules, the Cassie–Baxter state of a drop is transformed into the Wenzel state via the partial Wenzel state, with ethanol molecules filling the rough region, leading to an increase in its wettability. A linear relation of $1 + \cos \theta$ with the roughness parameter associated with the Cassie–Baxter and Wenzel states is observed, indicating that the solid–liquid interfacial tension is directly proportional to the roughness parameter. This behavior is akin to that seen for the case of pure liquid. The hydrogen bonding and density profile are analyzed to understand the wetting states of the blended drop.



1. INTRODUCTION

The role of wetting is important to characterize solid surfaces, which is relevant to both the natural world¹ and practical applications.² Numerous industrial, manufacturing, and biological applications require rapid wetting,^{3–5} whereas others demand poor wetting.^{6–8} Wettability is affected by a large number of factors such as the roughness of the surface, properties of the spreading liquid, presence of impurities, and material properties of the substrate.^{9–12} In recent years, both engineers and scientists have made greater efforts to understand wetting to obtain materials and surfaces with desired properties for engineering applications.^{1,13,14}

The wetting behavior of a liquid drop on a textured surface is commonly described by the Wenzel¹⁵ (water entering the spaces between protrusions) and Cassie–Baxter¹⁶ (water drop suspended on surface protrusions) models. Changing the roughness or texture of a surface is considered to be one of the methods for modifying its properties by lowering the surface energy,⁹ leading to a superhydrophobic surface. On the other hand, coating or chemically altering the surface or introducing a solute (surfactant) in the liquid can also modify the nature of wetting transitions. Considering the relevance of the latter case, various experiments on the wetting behavior of an aqueous surfactant drop on a substrate have been performed.^{17–20} In the presence of surfactant molecules, the wettability of a surface is modified due to the adsorption of the surfactant molecules at the liquid–vapor and liquid–solid interfaces, which modifies the interfacial tension.^{19,20} While the wetting transitions of pure liquid droplets on textured or chemically coated surfaces have been extensively studied, both theoretically and experimen-

tally,^{13,21–27} limited study has been done on the wetting transition of a blended liquid droplet on a solid surface,^{10,14,17,18,28,29} which is frequently encountered in many industrial applications, including agrichemical, textile, paint, ink, and biological systems. For example, an ethanol–water mixture has many practical applications in the medical, pharmaceutical, and chemical industries.^{30–32}

Although sparse, some efforts have been made to understand the molecular nature of blended liquids on surfaces using molecular simulation. For example, Lundgren et al.¹⁰ used molecular dynamics to investigate a water–ethanol drop on a substrate. They found that ethanol molecules prefer to remain close to the graphite surface. The wettability of an ethanol–water mixture was found to depend strongly on the ethanol concentration. However, no quantitative details were provided on the reorganization of water molecules in the presence of ethanol. Moreover, very few details are known about the hydrogen-bond (HB) network and its modification in the presence of ethanol. It is well-known that the surface tension of water is reduced by the adsorption of ethanol molecules on a liquid–vapor interface.³³ However, not much work has been done to understand the liquid–solid interfacial tension of water in the presence of alcohol. In addition, to the best of our knowledge, the line tension of the mixture, which may play an important role in the wetting of an ethanol solution at the nanoscale, is not known.

Received: September 27, 2013

Revised: January 10, 2014

Published: February 10, 2014

Recently, Boreyko et al.¹⁴ performed an experimental investigation to understand the wetting transition of an ethanol–water droplet on a superhydrophobic surface with hierarchical roughness. Two distinct wetting transitions were observed on the hierarchical surface with an increase in the ethanol concentration. The transition from the Cassie–Baxter state to the partial Wenzel state was found when ethanol molecules wet the microtiers. However, a transition from a partial Wenzel state to an impregnation state was found when the ethanol molecules wet the nanotiers. Though experiments have provided some insights for microscale and nanoscale rough surfaces with an increase in the ethanol concentration, it is not clear how wetting parameters such as the contact angle are related to the roughness parameters for the Cassie–Baxter and Wenzel states. Recently, Leroy et al.^{34,35} related the solid–liquid tension to the roughness parameter associated with the Cassie–Baxter and Wenzel states. In this work, we first investigate the line tension of an ethanol–water mixture on a smooth surface. The hydrogen bond distribution and density profiles are used to understand the self-assembly of the ethanol molecules on smooth and rough surfaces. Further, to demonstrate the extensibility of the observation for the pure system by Leroy et al., we adopt a simpler method using the contact angle on different rough surfaces to show that the reduced work of adhesion can be linearly associated with the roughness parameters corresponding to the Cassie–Baxter and Wenzel states.

The rest of the paper is organized as follows. In the next sections, we describe the model and methods employed in this work. Section IV presents the results and discussions followed by the conclusion in Section V.

II. MODEL AND METHODOLOGY

In this work, water is represented by the SPC/E water model.³⁶ The OPLS–AA model^{37–39} is employed for ethanol, as shown in eq 1

$$\begin{aligned}
 U = & \sum_{\text{bonds}} \frac{k_r}{2} (r - r_0)^2 + \sum_{\text{angles}} \frac{k_\theta}{2} (\theta - \theta_0)^2 \\
 & + \sum_{\text{dihedrals}} \sum_{n=1}^3 \frac{V_n}{2} [1 + (-1)^{n-1} \cos(n\varphi)] \\
 & + \sum_i \sum_{j \neq i} \left\{ 4\epsilon \left[\left(\frac{\sigma}{r_{ij}} \right)^{12} - \left(\frac{\sigma}{r_{ij}} \right)^6 \right] + \frac{1}{4\pi\epsilon_0} \frac{q_i q_j}{r_{ij}} \right\} \quad (1)
 \end{aligned}$$

where k_r and k_θ are the corresponding bond and angle force constants, and r and r_0 are the instantaneous and equilibrium values, respectively. θ and θ_0 are the instantaneous and equilibrium bending angles, respectively. V_n and φ are the Fourier coefficients and dihedral angle, respectively. The nonbonding parameters are the Lennard–Jones (LJ) diameter and energy well depth σ and ϵ , respectively; the partial atomic charges, q_i ; the atomic separation between atoms i , j , and r_{ij} ; and the dielectric permittivity constant, ϵ_0 .

The carbon–carbon nonbonded interactions for graphite are taken from Werder et al.⁴⁰ The nonbonded interactions are described in terms of the Lennard–Jones and Coulombic interaction, whereas the cross LJ interactions are described by the Lorentz–Berthelot geometric mixing rules. All of the interaction parameters are listed in Table S1 (Supporting Information).

The smooth graphite (111) surface consists of two layers of graphene (AB stacking) with hexagonally arranged carbon atoms, where the interlayer spacing and C–C bond distance are 3.4 and 1.42 Å, respectively. The lateral dimension of the simulation box is fixed to that of the surface dimension, which is varied from 150×150 to 200×200 Å², depending on the size of the ethanol–water droplet. The rough surface consists of two graphene layers as the base area, and the pillar height, h , varies with the number of graphene layers used. In this work, we use $h = 2, 4$, and 6 atomic layers of graphene sheets, corresponding to 6.8, 13.6, and 20.4 Å, respectively. Varying the pillar gap from 2.46 to 14.76 Å varies the roughness for a given pillar height. A schematic representation of the building block of the rough surface is shown in Figure 1. The surface fraction

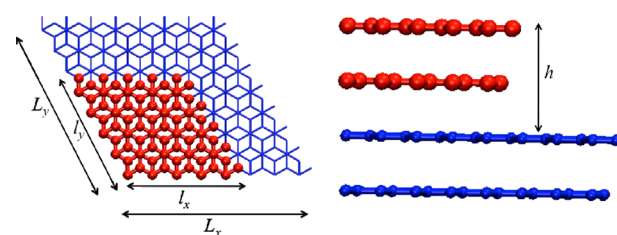


Figure 1. Schematic representations of side and top views of the unit cell of the pillared surface. The unit cell geometric parameters, L_x , L_y , and l_x , l_y are the lengths in the x and y directions of the base and pillar surface, respectively. h is the pillar height.

(α) is calculated from the ratio of the projected area of the pillar (A_p) to the base area (A_b), as given by the following relation

$$\alpha = \frac{A_p}{A_b} \quad (2)$$

The solid–liquid interfacial tension on surfaces with the Cassie–Baxter state for water droplets is shown to vary linearly in proportion to α . On the other hand, in the case of the Wenzel states, solid–liquid interfacial tension is shown to linearly depend on the ratio of the vertical groove area and the base area, defined as follows³⁵

$$\varphi = \frac{2(l_x + l_y)h}{L_x L_y} \quad (3)$$

The values of α and φ considered in this work are listed in Table 1.

Table 1. Dimensions of the Building Block for Rough Surfaces^a

dimensions of pillar, base layer (unit cell)	α	φ ($h = 2$)	φ ($h = 4$)
4, 10	0.160	0.442	0.885
5, 10	0.250	0.553	1.106
5, 8	0.390	0.864	1.728
5, 7	0.510		
5, 6	0.694		
11, 12	0.840		
10, 10	1.000		

^a α and φ are the surface fraction and surface heterogeneity factor, respectively. The pillar heights, $h = 2$ and 4 (i.e., 6.4 and 13.6 Å), correspond to two and four atomic layers for a graphene sheet, respectively.

Because the droplet size, in this work, is in the range of a few nanometers, the line tension plays an important role in the wetting behavior. Thus, the microscopic contact angle of the water–ethanol mixture can be described by the modified Young's equation.⁴⁰

$$\gamma_{SV} = \gamma_{SL} + \gamma_{LV} \cos \theta + \left(\frac{\tau}{r_b} \right) \quad (4)$$

where γ is the interfacial tension; the subscripts S, L, and V represent solid, liquid, and vapor, respectively; and θ is the microscopic contact angle of the droplet. τ and r_b are the line tension and base radius of the droplet, respectively. The macroscopic contact angle can be derived for an infinitely large drop, i.e., $1/r_b \rightarrow 0$, which yields a well-known Young's equation⁴⁰

$$\cos \theta_\infty = \left(\frac{\gamma_{SV} - \gamma_{SL}}{\gamma_{LV}} \right) \quad (5)$$

Equation 4 can be rewritten in terms of the macroscopic contact angle and line tension as shown below

$$\cos \theta = \cos \theta_\infty - \left(\frac{\tau}{\gamma_{LV}} \right) \frac{1}{r_b} \quad (6)$$

A series of finite size contact angles can be used along with eq 6 to obtain the macroscopic contact angle.

To determine the vapor–liquid densities and contact angles of a liquid droplet on a graphite surface, we adopt a graphical binning approach.^{21,40,41} We consider the cylindrical binning (r, z) of a droplet, assuming that it has azimuthal symmetry. Here, r is the distance from the z axis. We consider the topmost surface layer as the zero reference level and the surface normal through the center of the mass of the droplet as the reference axis. By imposing bins with a height of 1 Å parallel to the surface and equal volumes for all the elements, the i th radial bin is $r_i = (i\delta A/\pi)^{1/2}$ for $i = 1, \dots, N_{\text{bins}}$, where the fixed base area of each bin is $\delta A = 95 \text{ \AA}^2$. The z -density profiles are calculated across the center of mass of a droplet with a radius of 15 Å passing through the z axis. The positions of oxygen atoms of the water and ethanol are used to calculate the density of each bin. First, density profiles $\rho(r)$ across the vapor–liquid interface are fitted to a sigmoidal function²¹ to determine the location of the equimolar dividing surface. The vapor–liquid interface is considered to be located at the position where the density falls to half of its bulk density. Second, to extract the contact angle for a nanoscopic droplet, the best fit is found for a circle through these points of the vapor–liquid interface and extrapolated to a solid surface.

A binning procedure similar to that used for the density of the ethanol and water is applied to calculate the average number of hydrogen bonds (HBs) distributed within the droplet. Thus, two water molecules are hydrogen bonded if the following three conditions are satisfied:^{42,43} $R_{OO} < 3.5 \text{ \AA}$, $R_{OH} < 2.45 \text{ \AA}$, and $\text{HO}\cdots\text{O}$ angle $< 30^\circ$. A HB between any two molecules⁴⁴ (i.e., ethanol–ethanol, ethanol–water, or water–ethanol) exists if the following three conditions are satisfied: $R_{OO} < 3.5 \text{ \AA}$, $R_{OH} < 2.60 \text{ \AA}$, and $\text{HO}\cdots\text{O}$ angle $< 30^\circ$. The average number of HBs per water molecule is defined by the ratio of the total number of water–water and water–ethanol HBs formed to the total number of water molecules in each bin.

We define the average number of HBs per ethanol molecule in a similar way.

The wettability of the substrate can also be related to the work done by the energy per unit area, which is also referred to as the work of adhesion, as shown in the following Young–Dupre equation.⁴⁵

$$W_{\text{ad}} = \gamma_{LV}(1 + \cos \theta) \quad (7)$$

Further, the work of adhesion⁴⁵ is defined as the change in interfacial energy per unit area, which brings two interfaces from infinity to a certain distance and can be represented as

$$W_{\text{ad}} = \gamma_{SV} + \gamma_{LV} - \gamma_{SL} \quad (8)$$

Combining eq 7 and eq 8 yields the solid–liquid interfacial tension

$$-\gamma_{SL} = c + a(1 + \cos \theta) \quad (9)$$

where $c = -(\gamma_{SV} + \gamma_{LV})$ and $a = \gamma_{LV}$.

Therefore, the solid–liquid interfacial tension for a given state condition should be proportional to $1 + \cos \theta$. The linear variation of the solid–liquid free energy with the roughness parameters has been successfully reported for water.^{34,35} To understand the relation of the roughness and interfacial tension for a blended liquid on a textured surface, we study the reduced work of adhesion, $W_{\text{ad}}/\gamma_{LV} = W' = 1 + \cos \theta$, for various surface fractions and heterogeneity factors.

III. SIMULATION DETAILS

Molecular dynamic simulations are conducted at a constant particle number N , volume V , and temperature T (NVT ensemble) using the DLPOLY⁴⁶ (version 2.20) package. The cutoff distance for nonbonded interactions is set to 15 Å, and the long-range electrostatic interaction is calculated using the Ewald summation method.⁴⁷ The SHAKE algorithm is used to fix the bond length and angle for water molecules. All simulations are carried out at a temperature $T = 300 \text{ K}$. The ethanol concentration is varied in ranges of 0–30 wt % for a smooth surface and 0–75 wt % for pillared surfaces. At the start of the simulation, an equilibrated drop of the water and ethanol mixture is kept on the surface. The numbers of molecules are in the ranges of 2000–6000 for water and 83–2348 for ethanol as per the concentration. The size of the drop ranges from approximately 60 to 120 Å. Each simulation is carried out for $\sim 3 \text{ ns}$ with an integration time step of 1 fs, in which the last 500 ps is used to average over different properties. A Nosé–Hoover thermostat is used to maintain the system temperature with a relaxation constant of 1.0 ps. The surface is kept fixed at the bottom of the simulation box during all the simulations, and the height of the simulation box is taken to be 300 Å to avoid any interaction of periodic images of the droplet.

IV. RESULTS AND DISCUSSION

A. Wetting on Smooth Surface. We start our discussion with the structure and wetting behavior of ethanol–water droplets on a smooth graphite surface at different ethanol compositions. Figure 2 presents the z -density profile of ethanol–water droplets for 10, 20, and 30 wt % of ethanol. The local density, based on number density calculation, reveals the formation of water layers near the surface, with a density greater than the bulk density due to the influence of the substrate. The peak density progressively decreases with the distance from the surface, and at nearly 8 Å away from the

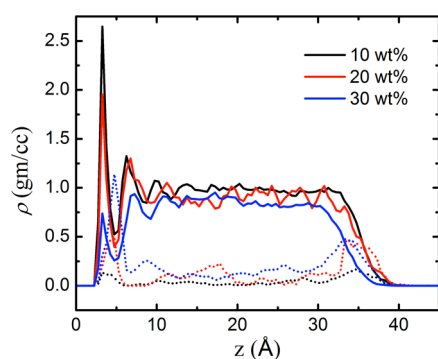


Figure 2. z -density profile of ethanol (dotted line) and water (solid line) along the centerline of the ethanol–water droplet on a smooth surface.

surface, the droplet approaches the bulk liquid density. Ethanol molecules preferentially adsorb either at the solid–liquid or vapor–liquid interface, as suggested by the peaks in the density profile. With increasing ethanol concentration, the water starts to deplete from the surface due to the preferential adsorption of ethanol. This is evident from the density of the first layer, which decreases with increasing ethanol concentration. At 30 wt % ethanol, the water density is lower than the bulk value, and the second layer density is much higher than that of the first layer. In the case of ethanol, the density in the first layer increases with the ethanol concentration. On the other hand, at the vapor–liquid interface, the ethanol density increases up to the 20 wt % ethanol solution and remains constant at approximately 0.5 g/cc at a higher weight percentage. On the other hand, this is not the case for the solid–liquid interface, where the ethanol density increases with the ethanol concentration. In general, the ethanol molecules accumulate at the solid–liquid and vapor–liquid interfaces with increasing ethanol composition. Figure 3 presents a contour diagram of

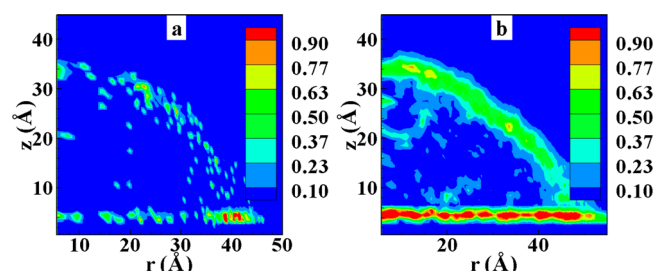


Figure 3. Contour plots of the average density profile of ethanol in an ethanol–water droplet on a smooth surface: (a) 10 wt % and (b) 30 wt %.

the average ethanol density. At 10 wt %, the majority of the ethanol molecules is located at the solid–liquid and liquid–vapor interfaces, with the maximum density at the three-phase contact line. With increasing concentration, the relative density of the ethanol at the solid–liquid interface is increased significantly. In contrast, the interfacial region of the vapor–liquid interface is broadened, although the peak density is not very sensitive to the concentration beyond 20 wt %. This is also supported by the broadened density region, for 30 wt % ethanol, around the density profile peak at the vapor–liquid interface, as shown in Figure 2, which is indicative of an increased interfacial thickness. Therefore, the ethanol molecules preferentially first accumulate at the three-phase contact line

and then at the two-phase solid–liquid and vapor–liquid interfaces.

To further understand the nature of the blended drop on the substrate, we analyzed the ethanol–ethanol, ethanol–water, water–water, and water–ethanol spatial HB distributions in detail (see Figure S3 of the Supporting Information). The average number of HBs, with the above criteria, in bulk water and ethanol is 3.63 ± 0.23 and 1.89 ± 0.25 , respectively. For the 10 wt % ethanol solution, the maximum number of HBs bonding due to ethanol molecules is found at the three-phase contact line, which is expected because this is where most of the ethanol molecules accumulate. Fewer hydrogen bonds due to ethanol molecules are found at the vapor–liquid and solid–liquid interfaces. As the ethanol concentration increases, the HB contribution due to ethanol molecules also increases at the vapor–liquid and solid–liquid interfaces. In the case of the 30 wt % ethanol solution, there are fewer HBs per water molecule close to the graphite surface compared to that in the bulk liquid droplet, where primarily it is water–water HBs. On the other hand, near the surface, the contribution from water–water HBs significantly decreases, due to the presence of a large number of ethanol molecules. Therefore, a complete network of ethanol molecules forms a cage-like structure around the droplet. However, the maximum number of HBs for ethanol is found close to the graphite surface, followed by the vapor–liquid interfacial region.

To see the effect of the ethanol concentration on the wettability of an ethanol–water droplet on a smooth surface, we estimate the contact angle. The contact angle depends on the size of the droplet, which is also seen for pure water droplets on a smooth graphite surface.^{41,48,49} Hence, we analyze the system size effect on the contact angle using 2000–6000 water molecules, where the number of ethanol molecules varies according to the concentration. Figure 4 shows the contact

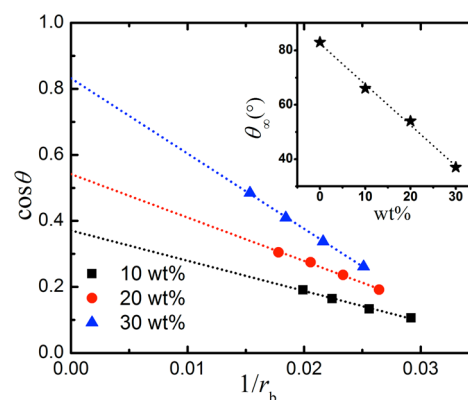


Figure 4. Dependence of system size on contact angle of the ethanol–water droplet on a graphite surface at different ethanol concentrations.

angle variation with the inverse of the base radius of the droplet. The contact angle of the ethanol solution is found to decrease with an increase in system size. The macroscopic contact angle of the droplet is estimated by extrapolating $1/r_b \rightarrow 0$, which is found to decrease with increasing ethanol concentration, in agreement with earlier studies.^{10,28} The macroscopic contact angle of the water droplet for this system is around 83° ,⁴¹ whereas for the 30 wt % ethanol solution it is $34 \pm 2^\circ$, as shown in the inset of Figure 4. Hence, the ethanol molecule clearly tunes the wetting behavior of the surface from hydrophobic to hydrophilic in nature, which was also observed

in a recent experimental study.¹⁴ The line tension is obtained by fitting the finite size contact angle data using eq 6, as shown Figure 4. From the slope, $-\tau/\gamma_{LV}$, and the surface tension value,³³ the line tension of the ethanol–water blend on the smooth graphite surface is calculated for different concentrations of ethanol. Table S2 (Supporting Information) lists the contact angle and line tension values for three concentrations. The order of the line tension values for different liquids varies widely, in the range of 10^{-12} to 10^{-6} N, as reported in the literature.^{50–52} The line tension, in this work, is on the order of 10^{-11} N for 0–30 wt % of ethanol. The order of this value is in line with earlier reported line tensions for water on a graphite surface.^{41,53} The vapor–liquid surface tension increases with an increase in the ethanol concentration.³³ Likewise, the line tension is found to increase with increasing concentration. This is not surprising, as it is known that line tension increases as a system approaches the complete wetting state.⁵⁴ This, for the pure liquid, is achievable with an increase in temperature.^{41,54,55} However, for a mixture, as in the current case, the same can be attained by increasing the solute (ethanol) concentration. At 300 K, the complete wetting state is achieved at an ethanol concentration of approximately 50 wt %.

B. Wetting on Textured Surface. Effect of Ethanol Concentration. Now, we turn our attention to the wetting behavior of ethanol–water droplets on rough surfaces. Figure 5

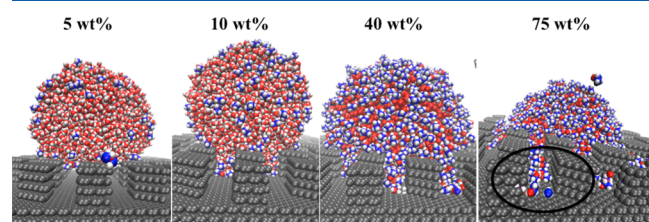


Figure 5. Configuration snapshots of the ethanol–water droplet on a rough surface ($h = 4$ and $\alpha = 0.25$) for different ethanol compositions: 5, 10, 40, and 75 wt %.

presents snapshots of ethanol–water droplets on a rough surface, for a fixed surface fraction ($\alpha = 0.25$) and pillar height ($h = 4$), with different ethanol concentrations. At 5 wt % ethanol, the drop is in the Cassie–Baxter state. With increasing ethanol concentration (to 10 and 20 wt %), a small amount of ethanol and water molecules penetrate into the grooves, leading to the partial wetting regime, as shown in Figure 5. A further increase in the ethanol concentration transforms the droplet to the fully Wenzel state due to an excessive number of ethanol molecules near the graphite surface. At a high ethanol concentration, 75 wt %, impregnation of the droplet (shown in circle) is observed. These wetting transitions with increasing ethanol concentration are in line with the results of a recent experimental study.¹⁴ Further, the apparent finite system size contact angles for different ethanol weight percentages are qualitatively in agreement with those of the experimental results (see Figure 6). The contact angle of a droplet on a rough surface depends on the system size as well as the wetting state of the droplet.^{24,56} Further, it may have hysteresis due to the pinning effect.⁵⁷ Our results show that the wetting transition of the ethanol–water droplet, with increasing ethanol weight percentage, is via the following path: Cassie–Baxter \rightarrow partial Wenzel \rightarrow Wenzel \rightarrow impregnation state.

Figure 7A presents the corresponding density contour plot with increasing ethanol concentration. For an ethanol

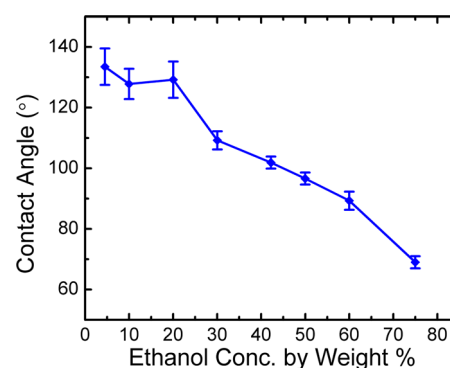


Figure 6. Contact angle as a function of ethanol concentration on a rough surface ($h = 4$ and $\alpha = 0.25$).

concentration of 0–5 wt %, the droplet is in the Cassie–Baxter state, and hardly any molecules penetrate inside the groove. With increasing ethanol concentration, ethanol molecules are predominant in the grooves, particularly near the groove surface. Further, the contour plots (see Figure 7A (c and d)) indicate that the ethanol molecules preferentially adsorb on the surface of the groove. In addition, ethanol molecules adsorb at the vapor–liquid interface, making a cage-like structure akin to that seen for a smooth surface. The water, on the other hand, is within the cage of ethanol molecules, as evident from Figure 7A (c and d). Figure 7B presents the HB distribution of the ethanol and water molecules, with increasing ethanol concentration. Figure 7B (c and d) shows that the ethanol–ethanol and ethanol–water HB networks are enhanced, with an increase in ethanol concentration, inside the groove, at the solid–liquid and vapor–liquid interfaces. On the other hand, the maximum number of water HBs is found in the bulk region of the drop, which diminishes with increasing ethanol weight percentage, as evident from Figure 7B (c and d). The results of the contour density profiles and HB distribution of ethanol molecules suggest that the ethanol concentration affects the wetting behavior, which is primarily due to the preferential adsorption at the interface.

Effect of Pillar Height. The height of the pillar plays an important role in the wetting of rough surfaces.²⁴ It has been found that a water drop prefers to stay in the Wenzel state at a lower pillar height, and there is a critical pillar height above which the Wenzel and Cassie–Baxter states can coexist.²⁴ However, this transformation is observed for a certain surface fraction range, which was extensively investigated in previous work.^{24,56} In this work, we have examined this transformation with the same system for 10 wt % of ethanol with varying pillar heights, as shown in Figure 8. We observe that the ethanol–water droplet is always in the Wenzel state at a pillar height $h = 2$, and a partial Wenzel state is found for $h = 4$, which is not seen for a pure water droplet.⁵⁶ To understand the reason for such a change in the wetting state with the pillar height, we study the density and HB distribution of ethanol and water (see Figure 4S of the Supporting Information). At a low pillar height, the highest density and HB of the ethanol molecules are found at the base layer of the substrate (see Figure 4S, Supporting Information). In contrast, the maximum water density and HB, as expected, are found in the center of the droplet. With increasing pillar height, the ethanol density increases at the solid–liquid and vapor–liquid interfaces. For $h = 2$, almost all the ethanol molecules wet the grooves, leading to the maximum density and HB near the surface. However, at

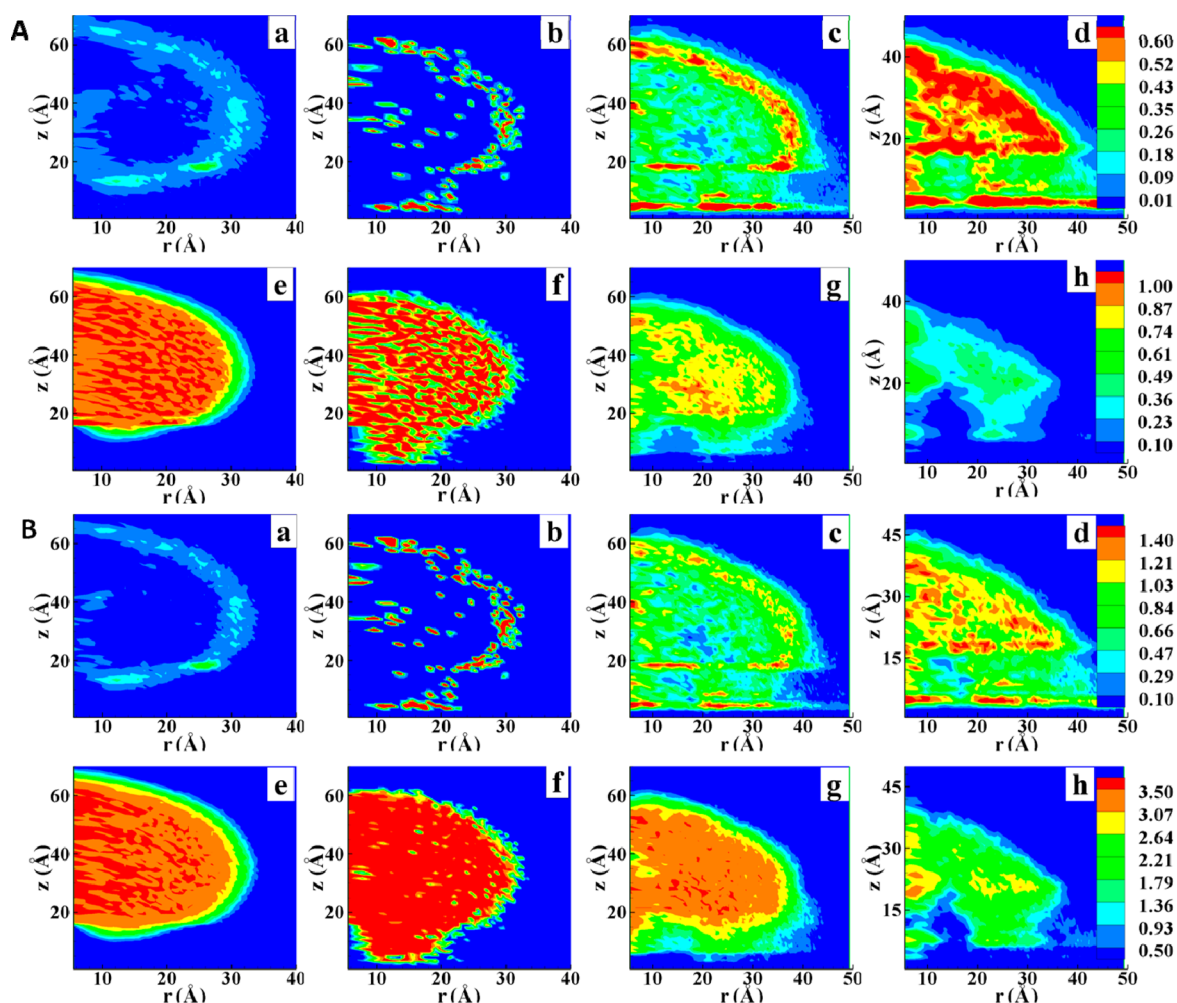


Figure 7. Density profile (A) of ethanol (a–d) and water (e–h) and average numbers of HBs (B) per ethanol (a–d) and water (e–h) molecules on a rough surface ($h = 4$ and $\alpha = 0.25$), for 5, 10, 40, and 75 wt % ethanol in an ethanol–water droplet. Here, $z = 0$ and 13.6 \AA are the tops of the base layer and pillar layer, respectively.

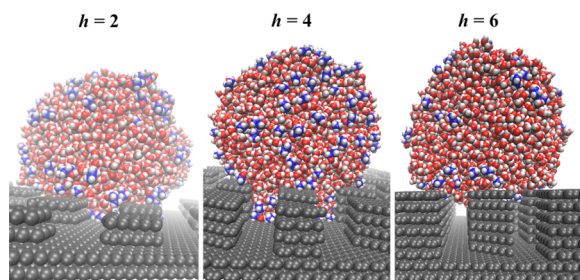


Figure 8. Configuration snapshots of an ethanol–water droplet (10 wt %) on rough surfaces, at surface fraction $\alpha = 0.25$, for $h = 2, 4$, and 6 .

$h = 4$, because of the significant barrier between the Cassie–Baxter and Wenzel states, while ethanol molecules still penetrate the grooves (though fewer in number), they are also found at the vapor–liquid interface. The drop still remains in the Wenzel state due to a sufficient number of ethanol molecules in the grooves. For $h = 6$, the barrier to the Wenzel state is increased significantly, and the droplet is found in the Cassie–Baxter regime. The effect of the pillar height on the wetting behavior of an ethanol–water droplet is summarized in Table 2. The ethanol molecules wet only the top solid surface and the vapor–liquid interfacial region. This significantly decreases the density and HBs of ethanol. In contrast, the

Table 2. Different Wetting States of Ethanol in the Ethanol–Water Droplet As a Function of Surface Fraction (α) and Pillar Height (h)

wt % ethanol	h	$\alpha = 0.25$	$\alpha = 0.39$	$\alpha = 0.51$
10	2	Wenzel	Wenzel	Cassie–Baxter
	4	Wenzel	-	-
	6	Cassie–Baxter	-	-
75	6	Wenzel	-	-
50	2	-	-	Wenzel

transition from the Wenzel state to the Cassie–Baxter state with increasing pillar height increases the density and HBs of water in the center of the drop (see Figure 4S, Supporting Information). The barrier to the Wenzel state due to the increased pillar height ($h = 6$) is found to decrease with the addition of more ethanol molecules, as observed for 75 wt % at $h = 6$, where a large amount of ethanol molecules penetrate into the grooves, as shown in Figure 5S (Supporting Information). We carefully examined the transformation and found that the ethanol molecules first enter the grooves of the rough surface, which helps water droplets to cross the energy barrier between the Cassie–Baxter state and the Wenzel state. This is also evident from Figure 5S(a) (Supporting Information), where the ethanol density in the groove at the base layer is very high and

the water density in that region is relatively low (as seen in Figure 5S(b), Supporting Information). Recently, Koishi et al.²⁸ investigated the behavior of a urea–water mixture on rough surfaces. The role of the urea molecules was just the opposite to that of the ethanol molecules. The urea molecules were found preferably near the graphite surface, as well as inside the droplet. However, there was no adsorption of urea molecules at the vapor–liquid interface. For rough surfaces, urea molecules were found to accumulate on the top of the pillar, which prevented the droplet from moving further into the grooves. There was also an increase in the free energy barrier between the Wenzel and Cassie–Baxter states with increasing urea concentration. On the other hand, ethanol molecules are found to accumulate preferably at the three-phase contact line and solid–liquid and vapor–liquid interfaces of the ethanol solution and are found to reduce the barrier between the Cassie–Baxter and Wenzel states.

Effect of Surface Fraction. It is now well understood that the ethanol molecules prefer to stay in the grooves for a lower pillar height ($h \leq 4$), as explained in an earlier section. Because ethanol molecules are less polar than water molecules, they have relatively more affinity to hydrophobic surfaces.⁵⁸ On the other hand, the size of an ethanol molecule is larger than that of a water molecule. Therefore, it is apparent that the spacing between pillars will have an important role in the wetting of rough surfaces. To clarify the above, we studied the wetting behavior of 10 wt % ethanol drops for different surface fractions ($\alpha = 0.25, 0.39, 0.51$) at a pillar height $h = 2$, as shown in Figure 9. When α is small, the groove width is greater than the pillar

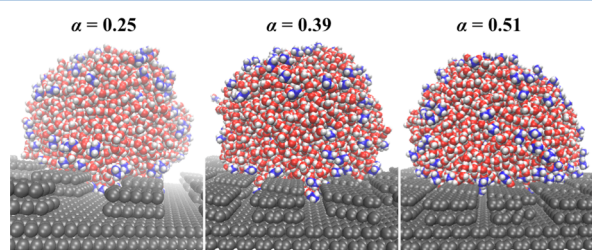


Figure 9. Configuration snapshots of an ethanol–water droplet (10 wt %) on rough surfaces at different surface fractions $\alpha = 0.25, 0.39,$ and 0.51 .

width, and a large number of molecules easily penetrate into the grooves. On the other hand, for large α , the amount of penetration is greatly reduced, which is well supported by the density and HB profile (not shown). For example, at a surface fraction $\alpha = 0.39$, the water droplet is in the partial Wenzel state,⁵⁶ whereas for a 10 wt % ethanol solution, it is in the Wenzel state. On the other hand, at a surface fraction $\alpha = 0.51$, the droplet with 10 wt % ethanol is in the Cassie–Baxter state, similar to that for the pure water case. This merely indicates that the ethanol weight percentage should be increased, at a higher surface fraction, to allow ethanol molecules to penetrate to change the wetting behavior of the rough substrate. To verify the above assertion, we enhanced the ethanol concentration to 50 wt %. The corresponding density and HB contour plots are shown in Figure 6S (Supporting Information). At this concentration, the ethanol molecules completely wet the base layer, as indicated by the increased density, which is even higher than the bulk ethanol density. The corresponding water density is found to be less at the solid–liquid and vapor–liquid interfaces. The HB distribution also indicates an extremely high

HB value for ethanol near the top solid–liquid interface, with penetration of the groove, which is not seen for the water molecules. Hence, the grooves mainly contain ethanol molecules. The HB distribution is in agreement with the density distribution (see Figure 6S(c and d), Supporting Information). The surface fraction effect on the wetting behavior of an ethanol–water droplet is summarized in Table 2. On the basis of the discussion of the effects of the surface fraction and pillar height, it is clear that the energy barrier between the Cassie–Baxter and Wenzel states can be modulated by the ethanol.

Work of Adhesion. Finally, we attempt to correlate the work of adhesion of the blended droplet with the roughness parameters of the surface. Recently, Leroy et al.^{34,35} studied the wetting behavior of water on a rough surface. They found that γ_{SL} is proportional to the surface fraction, α , for the Cassie–Baxter state and the surface heterogeneity factor, ϕ , for the Wenzel state. To understand the behavior of γ_{SL} for the blended liquid, we analyzed the reduced work of adhesion, $1 + \cos \theta$, as functions of γ_{SL} and ϕ for the Cassie–Baxter and Wenzel states, respectively. To illustrate the behavior of $1 + \cos \theta$, we consider the case of 10 wt % of ethanol. Further, the pillar height of the rough surface is fixed at either two or four graphene layers. Figure 10(a) represents $1 + \cos \theta$ vs α for the

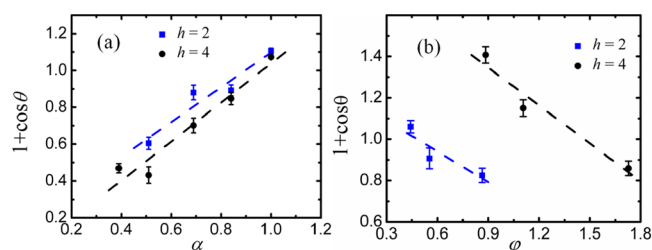


Figure 10. Reduced work of adhesion of a 10 wt % ethanol droplet with surface fraction (α) and surface heterogeneity factor (ϕ): (a) Cassie–Baxter States and (b) Wenzel states, for $h = 2$ and 4 .

Cassie–Baxter states. In case of the Wenzel states, the variations of $1 + \cos \theta$ with ϕ are plotted in Figure 10(b). It is observed that for both cases, i.e., the Cassie–Baxter and Wenzel states, the work of adhesion has a linear relationship with the respective roughness parameter, which is in agreement with the behavior seen for the pure system.^{34,35} This is also indicative of the linear relationships of the solid–liquid interfacial tension with α and ϕ for the Cassie–Baxter and Wenzel states, respectively. It should be noted that the deviation from the perfect linear relationship is mainly due to the error in representing the wetting states by the perfect Wenzel or Cassie–Baxter state. A direct calculation of the solid–liquid interfacial tension for the blended system is required to verify the observation seen in this work, which we plan to undertake in a subsequent work.

V. CONCLUSIONS

The effect of ethanol concentration on the wetting behavior of an ethanol solution on smooth and rough surfaces was investigated using molecular dynamic simulations. We observed that on smooth surfaces the ethanol molecules first accumulated at the three-phase contact line. Subsequently, they wet the vapor–liquid and solid–liquid interfaces with increasing ethanol concentration, which promoted the spreading of the droplet. The macroscopic contact angle of a droplet

was found to decrease with an increase in the ethanol concentration. On the other hand, the line tension increased with increasing ethanol concentration. However, the wetting behavior of the ethanol solution on a rough surface was quite different from that on a smooth surface. We studied the effects of the ethanol concentration, pillar height, and surface fraction on the wetting behavior of the solution. The microscopic contact angle of a droplet on a rough surface was found to decrease with an increase in the ethanol concentration. Therefore, our results indicated that ethanol molecules modify the wetting behavior of a surface from hydrophobic to hydrophilic in nature. We found that the microscopic contact angle on the textured surface was higher than that on a smooth surface at a given concentration of ethanol. Therefore, the roughness enhanced the surface hydrophobicity, and rough surfaces were better at resisting wetting by the ethanol–water droplet than smooth surfaces. For example, 50 wt % of ethanol was needed for complete wetting of the graphite surface. On the other hand, even 75 wt % of ethanol was not sufficient to wet the rough surface with $\alpha = 0.25$. The ethanol concentration required to transform the Cassie–Baxter state to the Wenzel state was found to depend on the surface fraction and pillar height. With increasing ethanol concentration, the sequence of wetting states was Cassie–Baxter \rightarrow partial Wenzel \rightarrow Wenzel \rightarrow impregnation state. The wetting transition and contact angle behavior with the ethanol concentration was in agreement with that seen in a recent experimental work. Finally, we found that the reduced work of adhesion was linearly proportional to the surface fraction and surface heterogeneity factor, for the Cassie–Baxter and Wenzel states, respectively.

■ ASSOCIATED CONTENT

● Supporting Information

The force field parameters, density and hydrogen bond distributions, and supporting table of contact angles and line tensions obtained in this work. This material is available free of charge via the Internet at <http://pubs.acs.org>.

■ AUTHOR INFORMATION

Corresponding Author

*E-mail: jayantks@iitk.ac.in.

Notes

The authors declare no competing financial interest.

■ ACKNOWLEDGMENTS

This research work was supported by the Department of Science and Technology (DST) and Council of Science and Industrial Research (CSIR), Government of India. The High Performance Computing (HPC) facility of Indian Institute of Technology Kanpur is gratefully acknowledged.

■ REFERENCES

- (1) Otten, A.; Herminghaus, S. How Plants Keep Dry: A Physicist's Point of View. *Langmuir* **2004**, *20*, 2405–2408.
- (2) Lavi, B.; Marmur, A. The Exponential Power Law: Partial Wetting Kinetics and Dynamic Contact Angles. *Colloids Surf., A* **2004**, *250*, 409–414.
- (3) López, V. H.; Kennedy, A. R. Flux-Assisted Wetting and Spreading of Al on TiC. *J. Colloid Interface Sci.* **2006**, *298*, 356–362.
- (4) Perelaer, J.; Hendriks, C. E.; de Laat, A. W. M.; Schubert, U. S. One-Step Inkjet Printing of Conductive Silver Tracks on Polymer Substrates. *Nanotechnology* **2009**, *20*, 165303.

- (5) Knoche, M. Organosilicone Surfactant Performance in Agricultural Spray Application: A Review. *Weed Res.* **1994**, *34*, 221–239.
- (6) Tuteja, A.; Choi, W.; Ma, M.; Mabry, J. M.; Mazzella, S. A.; Rutledge, G. C.; McKinley, G. H.; Cohen, R. E. Designing Superoleophobic Surfaces. *Science* **2007**, *318*, 1618–1622.
- (7) Roach, P.; Shirtcliffe, N. J.; Newton, M. I. Progress in Superhydrophobic Surface Development. *Soft Matter* **2008**, *4*, 224–240.
- (8) Chen, W.; Fadeev, A. Y.; Hsieh, M. C.; Öner, D.; Youngblood, J.; McCarthy, T. J. Ultrahydrophobic and Ultralyophobic Surfaces: Some Comments and Examples. *Langmuir* **1999**, *15*, 3395–3399.
- (9) Yoshimitsu, Z.; Nakajima, A.; Watanabe, T.; Hashimoto, K. Effects of Surface Structure on the Hydrophobicity and Sliding Behavior of Water Droplets. *Langmuir* **2002**, *18*, 5818–5822.
- (10) Lundgren, M.; Allan, N. L.; Cosgrove, T.; George, N. Wetting of Water and Water/Ethanol Droplets on a Non-Polar Surface: A Molecular Dynamics Study. *Langmuir* **2002**, *18*, 10462–10466.
- (11) Lin, C. T.; Lin, K. L. Contact Angle of 63Sn–37Pb and Pb-Free Solder on Cu Plating. *Appl. Surf. Sci.* **2003**, *214*, 243–258.
- (12) Kitajima, M.; Shono, T. Reliability Study of New SnZnAl Lead-Free Solders Used in CSP Packages. *Microelectron. Reliab.* **2005**, *45*, 1208–1214.
- (13) Miwa, M.; Nakajima, A.; Fujishima, A.; Hashimoto, K.; Watanabe, T. Effects of the Surface Roughness on Sliding Angles of Water Droplets on Superhydrophobic Surfaces. *Langmuir* **2000**, *16*, 5754–5760.
- (14) Boreyko, J. B.; Baker, C. H.; Poley, C. R.; Chen, C. H. Wetting and Dewetting Transitions on Hierarchical Superhydrophobic Surfaces. *Langmuir* **2011**, *27*, 7502–7509.
- (15) Wenzel, R. N. Resistance of Solid Surfaces to Wetting by Water. *Ind. Eng. Chem.* **1936**, *28*, 988–999.
- (16) Cassie, A. B. D.; Baxter, S. Wettability of Porous Surfaces. *Trans. Faraday Soc.* **1944**, *40*, 546–551.
- (17) Ivanova, N. A.; Starov, V. M. Wetting of Low Free Energy Surfaces by Aqueous Surfactant Solutions. *Curr. Opin. Colloid Interface Sci.* **2011**, *16*, 285–291.
- (18) Ivanova, N. A.; Zhantenova, Z. B.; Starov, V. M. Wetting Dynamics of Polyoxyethylene Alkyl Ethers and Trisiloxanes in Respect of Polyoxyethylene Chains and Properties of Substrates. *Colloids Surf., A* **2012**, *413*, 307–313.
- (19) Ferrari, M.; Ravera, F.; Liggieri, L. Preparation of a Superhydrophobic Surface by Mixed Inorganic–Organic Coating. *Appl. Phys. Lett.* **2006**, *88*, 203125.
- (20) Ferrari, M.; Ravera, F. Surfactants and Wetting at Superhydrophobic Surfaces: Water Solutions and Non Aqueous Liquids. *Adv. Colloid Interface Sci.* **2010**, *161*, 22–28.
- (21) de Ruijter, M. J.; Blake, T. D.; Coninck, J. D. Dynamic Wetting Studied by Molecular Modeling Simulations of Droplet Spreading. *Langmuir* **1999**, *15*, 7836–7847.
- (22) Gerdes, S.; Cazabat, A. M.; Ström, G.; Tiberg, F. Effect of Surface Structure on the Spreading of a PDMS Droplet. *Langmuir* **1998**, *14*, 7052–7057.
- (23) Cachile, M.; Bénichou, O.; Poulard, C.; Cazabat, A. M. Evaporating Droplets. *Langmuir* **2002**, *18*, 8070–8078.
- (24) Koishi, T.; Yasuoka, K.; Fujikawa, S.; Ebisuzaki, T.; Zeng, X. C. Coexistence and Transition Between Cassie and Wenzel State on Pillared Hydrophobic Surface. *Proc. Natl. Acad. Sci.* **2009**, *106*, 8435–8440.
- (25) Yong, X.; Zhang, L. T. Nanoscale Wetting on Groove-Patterned Surfaces. *Langmuir* **2009**, *25*, 5045–5053.
- (26) Ross, D.; Bonn, D.; Meunier, J. Observation of Short-Range Critical Wetting. *Nature* **1999**, *400*, 737–739.
- (27) Raj, R.; Maroo, S. C.; Wang, E. N. Wettability of Graphene. *Nano Lett.* **2013**, *13*, 1509–1515.
- (28) Koishi, T.; Yasuoka, K.; Zeng, X. C.; Fujikawa, S. Molecular Dynamics Simulations of Urea–Water Binary Droplets on Flat and Pillared Hydrophobic Surfaces. *Faraday Discuss.* **2010**, *146*, 185–193.

- (29) Ulman, A.; Evans, S. D.; Shnidman, Y.; Sharma, R.; Eilers, J. E. Mixed Alkanethiol Monolayers on Gold Surfaces: Wetting and Stability Studies. *Adv. Colloid Interface Sci.* **1992**, *39*, 175–224.
- (30) McDonnell, G.; Russell, A. D. Antiseptics and Disinfectants: Activity, Action, and Resistance. *Clin. Microbiol. Rev.* **1999**, *12*, 147–179.
- (31) Laizure, S. C.; Mandrell, T.; Gades, N. M.; Parker, R. B. Cocaethylene Metabolism and Interaction with Cocaine and Ethanol: Role of Carboxylesterases. *Drug Metab. Dispos.* **2003**, *31*, 16–20.
- (32) Hoogenboom, R.; Thijs, H. M. L.; Wouters, D.; Hoepfener, S.; Schubert, U. S. Tuning Solution Polymer Properties by Binary Water–Ethanol Solvent Mixtures. *Soft Matter* **2008**, *4*, 103–107.
- (33) Vázquez, G.; Alvarez, E.; Navaza, J. M. Surface Tension of Alcohol + Water from 20 to 50 °C. *J. Chem. Eng. Data* **1995**, *40*, 611–614.
- (34) Leroy, F.; Muller-Plathe, F. Rationalization of the Behavior of Solid–Liquid Surface Free Energy of Water in Cassie and Wenzel Wetting States on Rugged Solid Surfaces at the Nanometer Scale. *Langmuir* **2011**, *27*, 637–645.
- (35) Leroy, F.; Muller-Plathe, F. Can Continuum Thermodynamics Characterize Wenzel Wetting States of Water at the Nanometer Scale? *J. Chem. Theory Comput.* **2012**, *8*, 3724–3732.
- (36) Berendsen, H. J. C.; Grigera, J. R.; Straatsma, T. P. The Missing Term in Effective Pair Potentials. *J. Phys. Chem.* **1987**, *91*, 6269–6271.
- (37) Damm, W.; Frontera, A.; Tirado-Rives, J.; Jorgensen, W. L. OPLS All-Atom Force Field for Carbohydrates. *J. Comput. Chem.* **1997**, *18*, 1955–1970.
- (38) Jorgensen, W. L.; Maxwell, D. S.; Tirado-Rives, J. Development and Testing of the OPLS All-Atom Force Field on Conformational Energetics and Properties of Organic Liquids. *J. Am. Chem. Soc.* **1996**, *118*, 11225–11236.
- (39) Fern, J. T.; Keffer, D. J.; Steele, W. V. Vapor-Liquid Equilibrium of Ethanol by Molecular Dynamics Simulation and Voronoi Tessellation. *J. Phys. Chem. B* **2007**, *111*, 13278–13286.
- (40) Werder, T.; Walther, J. H.; Jaffe, R. L.; Halicioglu, T.; Koumoutsakos, P. On the Water–Carbon Interaction for Use in Molecular Dynamics Simulations of Graphite and Carbon Nanotubes. *J. Phys. Chem. B* **2003**, *107*, 1345–1352.
- (41) Dutta, R. C.; Khan, S.; Singh, J. K. Wetting Transition of Water on Graphite and Boron-Nitride Surfaces: A Molecular Dynamics Study. *Fluid Phase Equilib.* **2011**, *302*, 310–315; *ibid.* **2012**, *334*, 205.
- (42) Luzar, A.; Chandler, D. Hydrogen-Bond Kinetics in Liquid Water. *Nature* **1996**, *379*, 55–57.
- (43) Chandra, A. Effects of Ion Atmosphere on Hydrogen-Bond Dynamics in Aqueous Electrolyte Solutions. *Phys. Rev. Lett.* **2000**, *85*, 768–771.
- (44) Saiz, L.; Padró, J. A.; Guàrdia, E. Structure and Dynamics of Liquid Ethanol. *J. Phys. Chem. B* **1997**, *101*, 78–86.
- (45) Israelachvili, J. N. *Intermolecular and Surface Forces*, 3rd ed.; Academic Press: USA, 2011.
- (46) Smith, W.; Forester, T. R.; Todorov, I. T. *DL_POLY_2 User Manual*; STFC Daresbury Laboratory: Daresbury, Warrington WA4 4AD Cheshire, UK, 2009.
- (47) Allen, M. P.; Tildesley, D. J. *Computer Simulation of Liquids*; Clarendon: Oxford, 1989.
- (48) Scocchi, G.; Sergi, D.; D’Angelo, C.; Ortona, A. Wetting and Contact-Line Effects for Spherical and Cylindrical Droplets on Graphene Layers: A Comparative Molecular-Dynamics Investigation. *Phys. Rev. E* **2011**, *84*, 061602.
- (49) Vanzo, D.; Bratko, D.; Luzar, A. Wettability of Pristine and Alkyl-Functionalized Graphene. *J. Chem. Phys.* **2012**, *137*, 034707.
- (50) Amirfazli, A.; Neumann, A. W. Status of the Three-Phase Line Tension. *Adv. Colloid Interface Sci.* **2004**, *110*, 121–141.
- (51) Wang, J. Y.; Betelu, S.; Law, B. M. Line Tension Approaching a First-Order Wetting Transition: Experimental Results from Contact Angle Measurements. *Phys. Rev. E* **2001**, *63*, 031601.
- (52) Widom, B. Line Tension and the Shape of a Sessile Drop. *J. Phys. Chem.* **1995**, *99*, 2803–2806.
- (53) Ritchie, J. A.; Yazdi, J. S.; Bratko, D.; Luzar, A. Metastable Sessile Nanodroplets on Nanopatterned Surfaces. *J. Phys. Chem. C* **2012**, *116*, 8634–8641.
- (54) Szeleifer, I.; Widom, B. Surface Tension, Line Tension, and Wetting. *Mol. Phys.* **1992**, *75*, 925–943.
- (55) Joanny, J. F.; Gennes, P. G. D. Role of Long-Range Forces in Heterogeneous Nucleation. *J. Colloid Interface Sci.* **1986**, *111*, 94–101.
- (56) Khan, S.; Singh, J. K. Wetting Transition of Nanodroplets of Water on Textured Surface: A Molecular Dynamics Study. *Mol. Simul.* **2014**, *40*, 458–468.
- (57) Daub, C. D.; Wang, J.; Kudesia, S.; Bratko, D.; Luzar, A. The Influence of Molecular-Scale roughness on the Surface Spreading of an Aqueous Nanodrop. *Faraday Discuss.* **2010**, *146*, 67–77.
- (58) Hansford, D. T.; Grant, D. J. W.; Newton, J. M. Surface Energetics of the Wetting of a Hydrophobic Powder. *J. Chem. Soc., Faraday Trans. 1* **1980**, *76*, 2417–2431.